ACTA IMEKO
ISSN: 2221-870X
September 2026, Volume 15, Number 3, 1 - 6

Circularly polarized vision system for attenuation of reflection and glare

Luigi Montalto[1], Daniele Rinaldi[1], Paolo Castellini[2], Nicola Paone[2]

[1] *Dip. di Scienze e Ingegneria della Materia, dell'Ambiente ed Urbanistica, Università Politecnica delle Marche, Via Brecce Bianche 12- 60131 Ancona, Italy*
[2] *Dip. di Ingegneria Industriale e Scienze Matematiche, Università Politecnica delle Marche, Via Brecce Bianche 12- 60131 Ancona, Italy*

ABSTRACT
The paper presents the use of applying circular polarization in a vision system. It describes how reflections and glare are reduced when illuminating a reflecting surface with circularly polarized light and collecting scattered light through the same circular polarizer. Even if usage of linear polarizers in vision systems is common, the use of circularly polarized light offers advantages due to the simplicity of the setup, which is composed of a single polarizing plate, without any need for accurate angular alignment, enhancing the contrast without significant loss of illumination due to the absence of dark field regions. Reduction of glare reduces image saturation, therefore allowing for a better contrast in images acquired from highly reflective surfaces.

Section: RESEARCH PAPER

Keywords: vision system; polarization; glare; reflection; vision for measurement; measurement

Citation: L. Montalto, D. Rinaldi, P. Castellini, N. Paone, Circularly polarized vision system for attenuation of reflection and glare, Acta IMEKO, vol. 15 (2026) no. 3, pp. 1-6. DOI: 10.21014/actaimeko.v15i3.2169

Section Editor: Francesco Lamonaca, University of Calabria, Italy

Received August 11, 2025; **In final form** May 31, 2026; **Published** September 2026

Corresponding author: Luigi Montalto, e-mail: l.montalto@staff.univpm.it

1. INTRODUCTION

Vision systems are becoming ubiquitous, and many measurement systems are nowadays based on vision and image processing. Their use spans from industry to research and medicine with a large variety of optical layouts and image processing strategies [1]–[3]. Images can be considered data structures containing multiple information, which can be extracted by specific image processing algorithms [4]; they allow several quantities to be measured from a single image. For example, a simple 8-bit grey level image of a mechanical part placed on a conveyor contains geometric information, such as part dimensions and size, part shape, part position, part orientation, just to name a few. Spatial filtering, morphology, and blob analysis, or triangulation algorithms are usually capable of extracting geometry of the part [5], while matching algorithms, or more advanced artificial intelligence algorithms allow to recognize the part or to assess its conformity to specifications. Similarly, image analysis is used to detect surface defects in many applications [6], [7]. Examples of such use of imaging systems are state-of-the-art in industry, mainly for in-line quality control and part pick and place.

Despite the performance of the processing algorithm, a good measurement requires a good quality of the data, which, in case of vision systems, means a good quality of the image. Image quality generally implies no saturation and maximum contrast possible, as well as proper focus and depth of field. Saturation and contrast depend on illumination, surface scattering characteristics, camera optics, camera sensitivity, and exposure time. Illumination and camera parameters must be set properly with respect to the features and the details which have to be measured. Artifacts or disturbances, such as unwanted reflections, glare or saturated (dark or white) regions in the scene, should be reduced as much as possible, so as to enhance the signal-to-noise ratio of the image representing the data to be analysed. The design of the illumination system is therefore important to produce high-quality images [8]. Illumination is crucial for the improvement of image quality, and therefore to reduce the uncertainty of any further processing and measurement made on the image; parameters like spectral content [9], collimation, spatial distribution [10], [11], spatial structure, angular direction, and coherence and polarization need to be properly managed for each specific goal. In particular, light polarization is recognized as relevant when dealing with highly reflective surfaces [12] and for specific measurement methods [13], [14] in a number of different fields, such as industrial vision applications, material inspection, medicine, and environmental control.

Literature focuses on linearly polarized imaging, generally making use of crossed linear polarizers to eliminate undesired polarized reflections. However, most polarizers have the drawback of severe attenuation of image intensity and require an accurate angular alignment of the polarizer axes to be effective [15]. Linear polarization acquiring systems, such as polarized cameras, are nowadays available for vision and imaging application, with some limitation in resolution and sensitivity (specific or high-intensity illumination is needed) [16].

In this work, we focus instead on circular polarization, which, according to our knowledge, is not discussed in literature as a mean to improve contrast and reduce saturation. The advantage of circular polarization with respect to crossed linear polarizers is in terms of simplicity of the setup and reduction of the attenuation of intensity areas in the acquired scene.

Circular polarizers are used in photography and imaging for cutting the reflection of the external illumination in a specific layout, while in very few works, circular polarized illumination is used in combination with coherent light [17], such as in photoelasticity [18].

The method we propose makes use of a simple diffuse and uncoherent LED ring illuminator, equipped with a circular polarizer and a camera with camera optics collecting light in circular co-polarization conditions (through the same polarizer plate).

The paper is organized as follows: section 2 recalls the background theory of polarization, section 3 presents the method and the test setup, section 4 presents the results, and finally, section 5 draws the conclusions.

2. BACKGROUND THEORY ON POLARIZATION

In the framework of the Maxwell equations (as for this section, it is possible to refer to [19], [20]), the simple plane wave is composed by an electromagnetic field that propagates in the $\hat{s}$ direction in a Cartesian right-handed frame (x, y, z). The field $\vec{H}$ and $\vec{E}$ follow the condition

$$\vec{E} \cdot \hat{s} = \vec{H} \cdot \hat{s} = 0. \tag{1}$$

Moreover, $\vec{E}$, $\vec{H}$, and $\hat{s}$ form a right-handed vector triad. This means that the fields are in a plane normal to the propagation direction.

Light sources emit harmonic wave packets. For instance, we can describe a plane harmonic electromagnetic wave by means of the electric field vector propagating along x axis (with versor $\hat{s}$), having components:

$$E_y(x,t) = E_{y0} \sin(k\,x - \omega\,t)\,,$$

$$E_z(x,t) = E_{z0} \sin(k\,x - \omega\,t + \delta)\,, \tag{2}$$

where

$$\omega = k\,v = 2\,\pi\,f, \qquad \lambda\,f = v, \qquad k = \frac{2\,\pi}{\lambda}, \qquad \vec{k} = \frac{2\,\pi}{\lambda}\hat{s},$$

v is the wave velocity, λ is the wavelength.

We define the emitted light linearly polarized if the phase in equation (2) is $\delta = 0$ or $\delta = \pi$. In fact, equation (2) becomes:

$$E_y(x,t) = E_{y0} \sin(k\,x - \omega\,t)$$

$$E_z(x,t) = \pm E_{z0} \sin(k\,x - \omega\,t), \tag{3}$$

and finally, we obtain

$$\frac{E_z\,(x,t)}{E_y(x,t)} = \pm\,\frac{E_{z0}}{E_{y0}} = \tan\theta\,,$$

that is

$$E_z\,(x,t) = \tan\theta \cdot E_y(x,t). \tag{4}$$

Equation (4) is a straight line; this means that the polarization plane is the plane generated by the x axis and the line with an angle θ with respect to the plane (x, y). In this plane, the electric field has an amplitude of:

$$E_0 = \sqrt{E_{y0}^2 + E_{z0}^2}\,, \tag{5}$$

where $E_{y0} = E_0 \cos\theta,\ E_{z0} = E_0 \sin\theta$.

The case is different where the phase shift is either $\delta = \pi\,/\,2$ or $\delta = 3\,\pi\,/\,2$, equation (2) becomes

$$E_y(x,t) = E_{y0} \sin(k\,x - \omega\,t)$$

$$E_z(x,t) = \pm E_{z0} \cos(k\,x - \omega\,t) \tag{6}$$

Squaring and adding the equation (6) we obtain

$$\frac{E_y^2}{E_{0y}^2} + \frac{E_z^2}{E_{0z}^2} = 1\,. \tag{7}$$

Equation (7) means that the electric field describes an ellipse in the plane (y, z), as the magnitude of the electric field varies between E_{y0} and E_{z0}. In this case, we have the elliptic polarization. On the other hand, if $E_{y0} = E_{z0}$, the electric field rotates, describing a circle. This is the case of the circular polarization.

Now we consider what happens when a non-polarized (or a generally polarized) ray of light is reflected and refracted by a non-metallic (dielectric) surface. What follows can be easily demonstrated considering that the electric field component tangential to the boundary between the two surfaces is continuous across that boundary. We define the incidence plane as the plane generated by the vector $\vec{k}$ and the vector normal to the boundary surface $\hat{n}$ (plane π, that is the plane y-z, see Figure 1).

The refracted and reflected rays are partially polarized. At a particular incidence angle, $\theta_\mathrm{i} = \theta_\mathrm{p}$, the reflected ray is fully

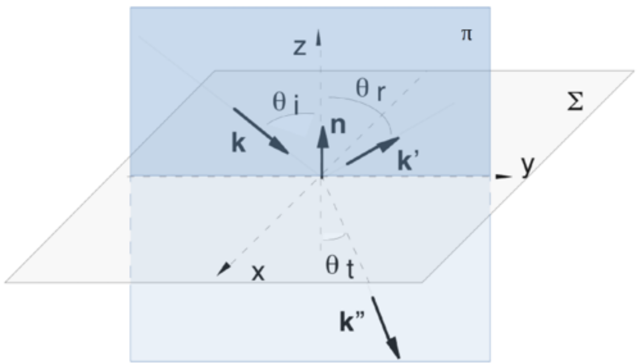

Figure 1. The plane Σ is the boundary between two dielectric surfaces (generally air and a non-metallic material). The incident reflected and transmitted (refracted) rays and angles are put in evidence (courtesy of [20]). The π plane $(y - z)$ is put in evidence.

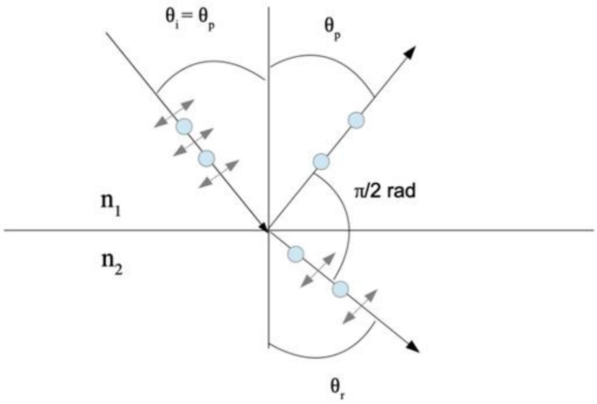

Figure 2. The impinging ray is not polarized (or generally polarized), the plane of the page is the π plane (incidence plane). The dots indicate the electric field vector component parallel to the Σ plane, the double arrows the electric field vector component parallel to the π plane.

polarized. In this case, the reflected light is polarized in a plane normal to the π plane (parallel to plane Σ), that is, the electric field is directed in a direction parallel to the reflecting surface. This phenomenon occurs when the refracted (transmitted) and the reflected rays are at $\pi/2$ rad (Figure 2).

So we obtain:

$$\theta_{\mathrm{p}} + \theta_{\mathrm{t}} = \pi/2 \,, \tag{8}$$

(the subscript t is for the refracted ray and $\theta_{\mathrm{i}} = \theta$, moreover, we remember that $\theta_{\mathrm{i}} = \theta_{\mathrm{r}}$), and using the Snell Law:

$$n_1 \sin\theta_{\mathrm{p}} = n_2 \sin\theta_{\mathrm{t}} \,,$$

$$n_1 \sin\theta_{\mathbf{p}} = n_2 \sin\left(\frac{\pi}{2} - \theta_{\mathbf{p}}\right) = n_2 \cos\theta_{\mathbf{p}}.$$

As a consequence, it results:

$$\frac{n_2}{n_1} = \frac{\sin\theta_{\mathrm{p}}}{\cos\theta_{\mathrm{p}}} = \tan\theta_{\mathrm{p}}. \tag{9}$$

The θ_{p} is called the Brewster angle, at this incidence angle, the reflected electromagnetic wave is totally polarized with the electric field entirely normal to the incidence plane π.

In an "ad hoc" frame, now we consider the case when the impinging electric field is polarized in the plane π (Figure 3a). Defining the reflectivity coefficient (r) as E_{r}/E_0 (where the subscripts indicate respectively the reflected and the incident electric field), we obtain:

$$r_{\pi} = \frac{E_{\mathrm{r}}}{E_0} = \frac{\tan(\theta_{\mathrm{i}} - \theta_{\mathrm{t}})}{\tan(\theta_{\mathrm{i}} + \theta_{\mathrm{t}})} = \frac{n_2\cos\theta_{\mathrm{i}} - n_1\cos\theta_{\mathrm{t}}}{n_2\cos\theta_{\mathrm{i}} + n_1\cos\theta_{\mathrm{t}}}. \tag{10}$$

Equation (10) evaluates the ratio between the reflected component of the electric field parallel to π to the impinging electric field. Equation (10) gives null result when $\theta_{\mathrm{i}} + \theta_{\mathrm{t}} = \pi/2$, that is the Brewster condition (8) and (9). It means that the electric field component parallel to π is completely transmitted at the Brewster incidence angle θ_{p} (Figure 3b).

In a very similar way, in the case when the incident wave is solely linearly polarized in a direction normal to the plane π (parallel to plane Σ, see Figure 4), we obtain that r_{Σ} is always not null, so the reflected wave is polarized in the plane parallel to Σ (tangential to the separation surface).

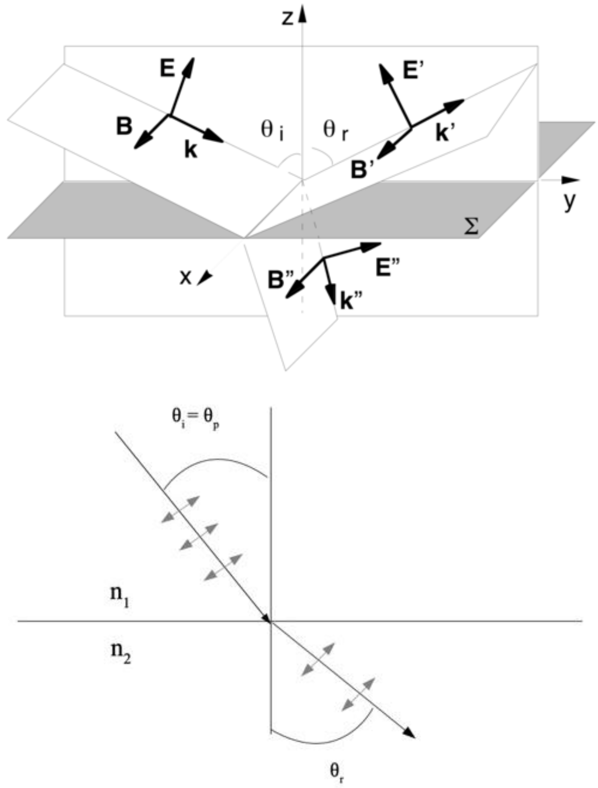

a)

b)

Figure 3. a) Reflection and refraction of an electromagnetic wave polarized in the plane π (courtesy of [20]), b) If $\theta_{\mathrm{i}} + \theta_{\mathrm{t}} = \pi/2$, the electric field is completely transmitted, and the reflected wave vanishes.

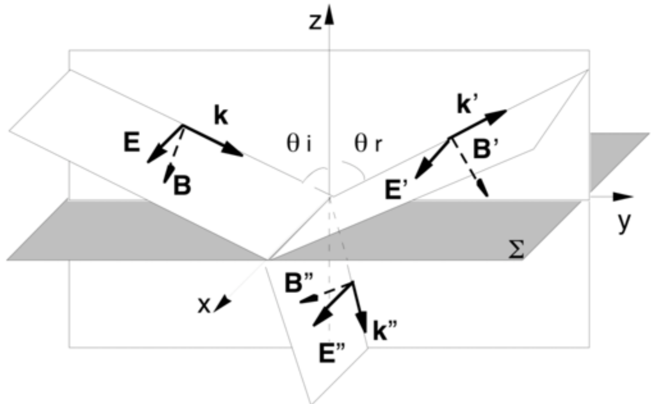

Figure 4. Reflection and refraction of an electromagnetic wave polarized in the plane parallel to Σ (courtesy of [20]).

3. EXPERIMENTAL METHOD

Referring to the previous section, according to some practical applications, when the Brewster condition is verified, it is possible to draw some conclusions: first of all, a generic polarized or unpolarized ray, at incidence angle θ_{p}, gives a reflected electric field polarized normal to the plane π. Meanwhile, the refracted electric field is a wave with the electromagnetic field directed both in the plane π and normal to it (Figure 2).

The component in the plane parallel to Σ is both reflected and transmitted (see Figure 4).

As a final remark, the most interesting case is when the impinging electric field has only the π component. In fact, at the θ_{p} incidence angle, the electric field is completely transmitted and no reflection is detected. On the contrary, the Σ component is both reflected and transmitted. The last conclusion is that in the reflected light, we find only light polarized in the plane parallel to Σ.

Now, if we consider a general curved surface (that admits the derivative and a tangent plane, π, in all the points), instead of a flat one, and an impinging light linearly polarized, it is possible, in same point (for instance, P_0) to be in the Brewster condition. So, in P_0, where the condition $\theta_\mathrm{i} + \theta_\mathrm{t} = \pi/2$ is verified, if the impinging light is polarized in the π plane (see Figure 3 and Equation 10) no reflections are detected.

Now we consider an impinging light that passes through a linear polarizer and a quarter plate, an elliptically polarized light is obtained (it means that the components in π and parallel to Σ planes are present, as the electric field rotates in the plane normal to the $\hat{s}$ direction). In this manner, a reflected ray is always present, also if the Brewster condition is verified in a certain point P_0 (see Figure 2). Considering a fixed detector, for the reflected light, composed by a quarter wave plate (with the axis rotated again of $\pi/4$) and a linear polarizer (with the same axis of the first linear polarizer), the result is that a light is detected in every point including P_0. In fact, in P_0, the quarter wave plate transforms the reflected linear polarized light in the plane π into an elliptically polarized light that can be detected by the linear polarizer of the detector. If we are not in P_0 (Brewster condition), the reflected wave is also elliptically polarized. The quarter wave plate introduces again a $\pi/4$ phase shift and the light that can be detected by the final linear polarizer, except in the case of direct reflection, that is the extinction case. This layout can detect the light in every point, also in P_0, and contemporarily partially reduces, owing to the final polarizer, the reflected light.

A circular polarizer plate is an optical component composed by a linear polarizer and a $\lambda/4$ waveplate with its fast and slow axes at 45° with respect to the linear polarizer. The two components are joined together in a sandwich; therefore, they constitute a single optical element.

A monochromatic industrial camera has been provided with a LED light, so as to have a quasi-coaxial illumination along the lens optical axis.

A circular polarizer plate is placed in front of the illuminator and the camera; this arrangement makes the light projected onto the target surface to be circularly polarized. When a circular polarized light is back scattered by a surface, the polarization of the reflected part tends to remain circular as long as the impinging angle is far from the Brewster angle. The back reflected light will have a circular polarization with opposite rotation with respect to the impinging one; this condition leads to the elimination or strong attenuation of the back reflected light by the circular polarizing element in front of the camera.

On highly reflecting surfaces, direct reflections tend to saturate the image or to reproduce on the detector the image of the illuminator itself, compromising the quality of the acquired scene; features are masked by the saturation and by the direct reflections. Therefore, the drastic reduction of reflections produced by the circular polarization arrangement is a valuable solution to improve image quality, that is, the signal-to-noise ratio.

An experimental setup has been arranged acquiring images of two high-reflecting samples:

1. A polymeric packaging with a reflecting holographic surface.
2. An aluminium plate with a semi-polished surface.

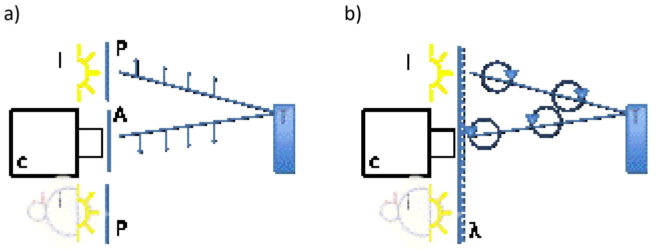

Figure 5. The two optical layouts: a) crossed polarizers (P and A respectively); b) a single circular polarizer plate λ.

These two surfaces represent two examples of large industrial interest, the first one concerning the packaging sector, the second one the metal industry.

For comparison purposes, the same scene has been acquired in three different conditions:

1. no polarizing optics,
2. linear polarization for both illumination and camera lens in cross-polarization condition (see Figure 5 a),
3. circular polarization condition with illumination and camera lens in co-polarization layout (see Figure 5 b).

The samples have been acquired placing them on two different supports (white and black) for evaluating the reduction of the glare and the disturbance provided by the support.

The scheme in Figure 5 a represents the linear cross polarized system: the illumination (i) is linearly polarized by the polarizer (P); the surface direct reflections, from the target (T), will maintain the linear polarization, the camera (C) will not be affected by those reflections due to the analyser (A), a crossed polarizer with respect to (P).

In Figure 5 b, the right P and A are substituted by a unique component (λ) which circularly polarizes the light. Direct reflections are still circularly polarized but counter rotating with respect to the original light rays, therefore this reflected light will not pass through the circular polarizer (λ); so the camera (c) will not be blinded by those reflections. Besides the other advantages with respect to the system on the left, the simplification of the circular polarizing setup is evident: no need for optical alignment (while system 1 needs a proper alignment for crossing the polarizers at 90°) and a single component for the light illumination and camera acquisition polarization. Arrows and dots on the light ray are representing the polarization components.

4. RESULTS AND DISCUSSION

The images on the polymeric packaging reported in Figure 6 a, b, c, have been acquired by an industrial camera with a fixed integration time. In particular, Figure 6 a without any polarization; Figure 6 b in linear cross-polarization layout; Figure 6 c in circular co-polarization.

The images of the aluminium plate reported in Figure 6 d, Figure 6 e, and Figure 6 f have been acquired with a USB camera (webcam) in auto exposure mode. In particular, Figure 6 d without any polarization; Figure 6 e in linear cross-polarization strategy; Figure 6 f in circular polarization co-polarization.

By considering the acquired images, the enhancement of contrast and reduction of saturation when using polarizing elements is clear with respect to the images acquired with unpolarized illumination (Figure 6 a and d).

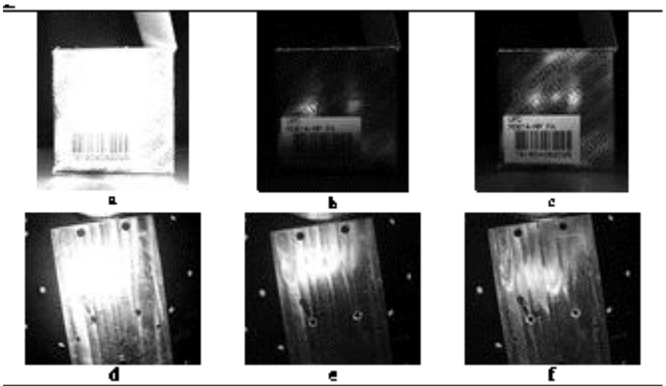

Figure 6. Set of acquired images. The images a (no polarization), b (linear polarization), c (circular polarization) are acquired by the industrial camera with a constant exposure. The images d (no polarization), e (linear Polarization), f (circular polarization) are acquired by a webcam in auto exposure mode.

In the case of the polymeric packaging, the high reflectivity of the surface produces a completely saturated image if no polarizers are used.

Crossed linear polarizers are effective in reducing glare and saturation; however, the average intensity of the image decreases, due to the possible dark field condition in cross polarization setup with the linear polarizers. When considering the image obtained by using the circular polarizer, we observe the significant reduction of glare and saturation and an average image intensity larger than the one with crossed polarizers (see Figure 6 and Figure 7). Overall, when using a single circular polarizer, the problem of image saturation is solved, keeping a sufficiently high contrast. In fact, due to the circular polarization, completely dark field (which can mask features in the scene) is avoided.

In the case of the aluminium metal plate, a similar effect is observed. It is important to note that in this case the camera was operated in auto-exposure mode. Therefore, all the images have an intensity which spans across the entire 8-bit levels. The amount of glare, and the contrast and readability of the scene is best when using the circular polarization, which, even in this case, provides reduction of saturation and optimal contrast.

The benefit of the circular polarization setup is confirmed by the simple analysis of the histograms of the scene; Figure 7 shows the comparison of the histograms between images acquired by the linear and the circular polarizing layout. The general benefits, which are linked to the proposed method, are paid with a lower brightness resulting in a darker scene; however, with critical surface conditions, such as high-reflecting finishing, mirror-like surfaces and features, or deposited thin films, a strong improvement (e.g. histogram equalization, contrast-to-noise ratio, and general features detectability in the scene) is obtained. For example, the contrast-to-noise ratio (CNR) increases from the linear polarized system to the circular polarised (and, of course, from the completely saturated scene of the system without any polarization). In our cases, the CNR, in the barcode of the images in Figure 6, spans from 27 to 32 using circular polarization, while in the linear polarization systems, it goes from 1.5 (dark region) to 24 (brighter side). Due to the saturated scene, unmeaningful CNR values are related to the non-polarized system; in fact, features are completely undetectable due to the blinding reflections.

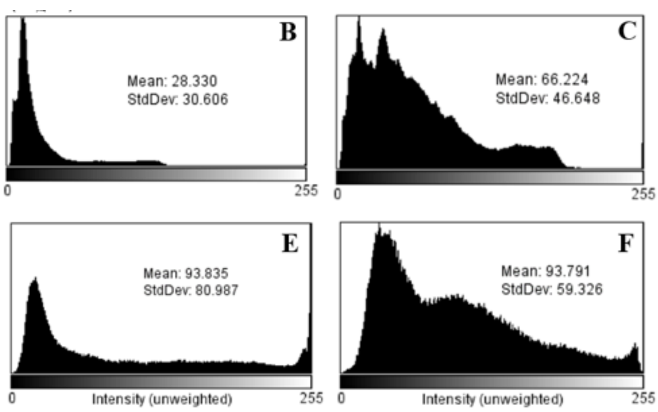

Figure 7. The resulting normalized histograms of the images B, C, E, and F. Besides the elimination of the saturated part of the images, it is worth noting that, in the images C and F (with the circular polarization), the histogram is more homogeneous; the number of pixels with an average illumination is higher. Therefore, extremely dark regions and saturation are reduced by using the circular polarization setup. In the insets, the intensity mean value and its standard deviation are presented.

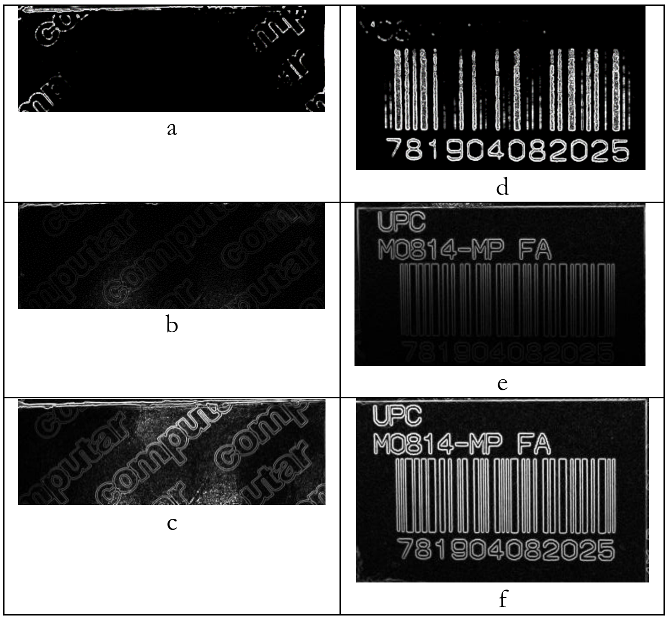

Figure 8. The results of the edge detection algorithm applied on the box shown in Figure 6 are presented: a, b, c are the upper part of the box acquired respectively under no-polarization (a), linear polarization (b), and circular polarization (c) conditions; d, e, f are the barcode side of the box acquired under no-polarization (d), linear polarization (e), and circular polarization (f) conditions.

The effect is considerable in both non-metallic and metallic surfaces, a slightly stronger in this last class due to their conductive nature, which reduces the reflectionless at the Brewster angle, in fact bringing to a pseudo-Brewster angle/effect [19].

The enhancement of the quality of the scene detection due the circular polarization setup is clear even using a standard edge detection algorithm (e.g., using the standard edge detection plug of ImageJ from Wayne Rasband of the National Institute of Health, USA), see Figure 8.

From the images in Figure 8, the vision system provided with circular co-polarization system shows enhanced capability in detecting features and information in the scene with respect to the other systems, in which the information is degraded by saturated or too dark areas in the images. In fact, both the barcode and the box stamp are correctly detected by the circular polarised system, while they are entirely or partially missed when acquired with the non-polarized or linearly polarized system.

Table 1. Pros and cons of the different approaches.

	No polarisation	Linear polarisation	Circular polarisation
Blinding reflection and glare reduction	×	√	√
Contrast enhancement	×	√	√
Illumination intensity	√	×	√
Ease of implementation	√	×	√

Moreover, it is important to observe that, while setting up the crossed linear polarized system, particular care was necessary for properly aligning the polarizers at 90° to each other, arranging the circular polarized equipment was extremely less complex due to the presence of a unique optical element which does not need for any alignment.

Table 1 reports a summary of pros and cons of the three imaging system schemes that have been compared, with regard to:

- Effect on saturation;
- Contrast enhancement;
- Average intensity attenuation;
- Ease of implementation in terms of alignment and setup arrangement.

The circular polarization scheme has some advantages with respect to the crossed polarizers.

5. CONCLUSIONS

As already known from literature, when using polarization, we observe a strong reduction of saturation due to reflections and glare. By using a circular polarizer operated in co-polarization, both on the illumination and on the receiving optics, image quality is enhanced with respect to using crossed linear polarizers only. This is due to the fact that the co-polarization in the circular polarizing setup led to a reduction of the saturation relative to the direct reflection, which are still circularly polarized but counter rotating; in parallel, the average illumination is maintained, and an optimal contrast is obtained, avoiding dark field region typical of the crossed polarized setups. Furthermore, the system is strongly simplified; in fact, no alignment is needed for the circular co-polarization setup, since a unique optical element is used, while aligning crossed polarizers is crucial.

REFERENCES

[1] M. A. Montironi, P. Castellini, L. Stroppa, N. Paone, Adaptive autonomous positioning of a robot vision system: Application to quality control on production lines, Robotics and Computer-Integrated Manufacturing 30 (2014) 5, pp. 489–498.
DOI: 10.1016/j.rcim.2014.03.004

[2] P. Catti, M. Ntoulmperis, V. Medici, M. Martarelli, N. Paone, W. van de Kamp, N. Nikolakis, K. Alexopoulos, Quality control in manufacturing through temperature profile analysis of metal bars: A steel parts use case, Procedia CIRP 129 (2024), pp. 205–210, ISSN 2212-8271.
DOI: 10.1016/j.procir.2024.10.036

[3] P. Castellini, M. A. Montironi, A. Zizzi, M. Scarpelli, R. Mazzucchelli, A. Lopez-Beltran, L. Cheng, N. Paone, (+ 1 more author), Recurrent papillary urothelial neoplasm of low malignant potential. Subtle architectural disorder detected by quantitative analysis in DAXX-immunostained tissue sections, Human Pathology 45 (2014) 4, pp. 745–752, ISSN 0046-8177.
DOI: 10.1016/j.humpath.2013.10.034

[4] J. Xiao, Z. Sun, H. An, H. Zhao, M. Qiu, X. Li, Optical image processing and applications empowered by vision-language models, iOptics 1 (2025) 1, 100003, ISSN 3051-1771.
DOI: 10.1016/j.iopt.2025.100003

[5] G. Di Leo, C. Liguori, A. Paolillo, A. Pietrosanto, Machine vision systems for on line quality monitoring in industrial applications, Acta IMEKO 4 (2015) 1, pp. 121–127.
DOI: 10.21014/acta_imeko.v4i1.176

[6] K. Trambitckii, K. Anding, G. Polte, D. Garten, V. Musalimov, P. Kuritcyn, The application of texture features to quality control of metal surfaces, Acta IMEKO 5 (2016) 4, pp. 19–23.
DOI: 10.21014/acta_imeko.v5i4.415

[7] Z. Ren, F. Fang, N. Yan, Y. Wu, State of the Art in Defect Detection Based on Machine Vision. Int. J. of Precis. Eng. and Manuf.-Green Tech. 9 (2022), pp. 661–691.
DOI: 10.1007/s40684-021-00343-6

[8] S. K. Kopparapu, Lighting design for machine vision application. Image and Vision Computing 24 (2006) 7, pp. 720–726.
DOI: 10.1016/j.imavis.2005.12.016

[9] M. Lee, D. Seo, B. Seo, J. Park, Optimal illumination for discriminating objects with different spectra, Opt. Lett. 34 (2009), pp. 2664–2666.
DOI: 10.1364/OL.34.002664

[10] P. Castellini, S. Cecchini, L. Stroppa, N. Paone, Adaptive illumination through spatial modulation of light intensity and image inversion, Measurement Science and Technology 24 (2013) 5, 055401.
DOI: 10.1088/0957-0233/24/5/055401

[11] P. Castellini, S. Cecchini, L. Stroppa, N. Paone, Optimization of spatial light distribution through genetic algorithms for vision systems applied to quality control, Measurement Science and Technology 26 (2015) 2, art. No. 025401.
DOI: 10.1088/0957-0233/26/2/025401

[12] S. G. Demos, R. R. Alfano, Optical polarization imaging, Appl. Opt. 36 (1997), pp. 150–155.
DOI: 10.1364/ao.36.000150

[13] L. Montalto, D. Rinaldi, L. Scalise, N. Paone, F. Davì, Photoelastic sphenoscopic analysis of crystalsRev. Sci. Instrum. 87 (2016), art. No. 015113.
DOI: 10.1063/1.4940196

[14] L. Montalto, P. P. Natali, F. Daví, P. Mengucci., N. Paone, D. Rinaldi, Characterization of a defective $PbWO_4$ crystal cut along the a-c crystallographic plane: structural assessment and a novel photoelastic stress analysis, JINST 12 (2017) 12, P12035.
DOI: 10.1088/1748-0221/12/12/P12035

[15] J. del Hoyo, A. Soria-Garcia, J. Andres-Porras, J. Alda, L. M. Sanchez-Brea, High accuracy and precision measurement method of the extinction coefficient and retardance of non-perfect linear polarizers, Measurement 256 (2025), art. no118190.
DOI: 10.1016/j.measurement.2025.118190

[16] L. Chiominto, G. D'Emilia, E. Natale, A. Stamopoulos, Uncertainty evaluation of composite inspection methods based on the use of polarized camera, Measurement: Sensors 38 (2025), art. No. 101595.
DOI: 10.1016/j.measen.2024.101595

[17] R. A. Chipman, W. S. T. Lam, G. Young, Polarized Light and Optical Systems, CRC Press Taylor & Francis Group, 2018, Boca Raton London New York, ISBN: 9781351129121.

[18] J. W. Dally, W. F. Riley, Experimental Stress Analysis, McGraw-Hill, 1978, London.

[19] M. Born, E. Wolf, Principles of Optics, Pergamon Press, Oxford 1970.

[20] R. G. M. Caciuffo, S. Melone, Fisica Generale, Vol. II, Masson, Milano, 1997. [In Italian]